Theory of topological corner state laser in Kagome waveguide arrays

Cite as: APL Photon. 6, 040802 (2021); doi: 10.1063/5.0042975
Submitted: 5 January 2021 • Accepted: 8 April 2021 •
Published Online: 21 April 2021

Hua Zhong,[1] Yaroslav V. Kartashov,[2,3] Alexander Szameit,[4] Yongdong Li,[1] Chunliang Liu,[1] and Yiqi Zhang[1,a)]

AFFILIATIONS

[1] Key Laboratory for Physical Electronics and Devices of the Ministry of Education & Shaanxi Key Lab of Information Photonic Technique, School of Electronic and Information Engineering, Xi'an Jiaotong University, Xi'an 710049, China
[2] ICFO-Institut de Ciències Fotòniques, The Barcelona Institute of Science and Technology, 08860 Castelldefels, Barcelona, Spain
[3] Institute of Spectroscopy, Russian Academy of Sciences, Troitsk, Moscow 108840, Russia
[4] Institute for Physics, University of Rostock, 18059 Rostock, Germany

Note: This paper is part of the APL Photonics Special Topic on Synthetic Gauge Field Photonics.
[a)] **Author to whom correspondence should be addressed:** zhangyiqi@mail.xjtu.edu.cn

ABSTRACT

In comparison with conventional lasers, topological lasers are more robust and can be immune to disorder or defects if lasing occurs in topologically protected states. Previously reported topological lasers were almost exclusively based on the first-order photonic topological insulators. Here, we show that lasing can be achieved in the zero-dimensional corner state in a second-order photonic topological insulator, which is based on the Kagome waveguide array with a rhombic configuration. If gain is present in the corner of the structure, where the topological corner state resides, stable lasing in this state is achieved, with the lowest possible threshold, in the presence of uniform losses and two-photon absorption. When gain acts in other corners of the structure, lasing may occur in edge or bulk states, but it requires substantially larger thresholds, and transition to stable lasing occurs over much larger propagation distances, sometimes due to instabilities, which are absent for lasing in corner states. We find that increasing two-photon absorption generally plays strong stabilizing action for nonlinear lasing states. The transition to stable lasing stimulated by noisy inputs is illustrated. Our work demonstrates the realistic setting for corner state lasers based on higher-order topological insulators realized with waveguide arrays.

I. INTRODUCTION

Generally, a d-dimensional (dD) topological insulator supports (dD) bulk states and ($d-\ell$)D topological edge states. First-order TIs correspond to $\ell = 1$, while for higher-order topological insulators (HOTIs), one has $\ell > 1$.[1,2] Nowadays, HOTIs attract considerable attention in diverse areas of physics, as they were discovered in condensed matter physics,[3–10] electrical systems,[11] mechanical systems,[12,13] acoustics,[14–17] microwave systems,[18] and photonics.[19–26] Different from first-order topological insulators that satisfy the bulk–edge correspondence principle,[27,28] HOTIs do not comply with this principle, even though they support topologically protected states.[14,15] The simplest realization of a HOTI is a 2D insulator supporting 0D topological corner states. As $\ell = 2$, such a system is called second-order topological insulator HOTIs that were reported not only in conservative systems but also in non-Hermitian settings.[29–32] Only recently HOTIs with nonlinearity-dependent hopping rates that enter the topological phase at high enough amplitudes[33] have been considered theoretically, while coupling between corner modes in nonlinear HOTIs in polariton systems has been addressed in Ref. [34].

Nonlinear effects are imperative for implementing laser systems. Nonlinearity leads to competition between different lasing modes, as a result of which only a limited set of them survives, leading to substantial modification of the output spectrum in the stable lasing regime. Gain saturation, accounted for by nonlinear terms in

the corresponding governing equations, determines the amplitudes of lasing modes. These effects were employed for the realization of so-called topological lasers[35–41] representing a novel extension of the concept of topological insulators. In comparison with conventional lasers, whose stability may be affected by perturbations, such as defects and disorder, topological lasers may be more stable when they lase in topologically protected edge states. Topological lasing has been theoretically proposed and experimentally reported in the 1D systems representing variants of the Su–Schrieffer–Heeger (SSH) lattices[35–38] and in fully 2D settings based on topological photonic crystals[42] and lattices of coupled-ring resonators.[43,44] Lasers based on the valley Hall effect were reported in Refs. 45–48. Topological lasing is possible in Floquet topological insulators,[49] and it was proposed using the bosonic Harper–Hofstadter model.[50] In polariton systems, topological lasing in the 1D and 2D microresonator arrays has been demonstrated experimentally[36,51] and studied theoretically when sufficiently strong pump and, in some cases an external magnetic field, was provided in the system.[52]

Remarkably, in all previous works, even those addressing finite topological configurations,[53] lasing in 2D systems was shown to occur in the extended edge states, typically along the entire periphery of the insulator.[42–44] In contrast, HOTIs potentially allow the realization of a class of higher-order topological lasers, where despite the fact that the system will still show fully two-dimensional evolution, lasing will occur in localized 0D corner modes, enabling high spatial localization of the emission and its constant modal population (in a sense that only one nonlinear mode will be excited above the lasing threshold). In addition, corner lasers constructed on topologically protected edge states should exhibit benefits of topological protection of lasing. This is because corner states always survive even for harsh perturbations in the bulk of the photonic lattice because topological properties are not destroyed unless perturbation-induced shifts of propagation constants exceed the width of the topological gap.

The goal of this work is to demonstrate that a corner laser can be implemented in a new continuous system, which is based on Kagome[14,15,22,54] waveguide arrays, where localized gain can be selectively provided in different waveguides of the array and where uniform losses, two-photon absorption, and focusing nonlinear interactions are present. Even though lasing in 0D corner states has been recently reported in photonic crystal cavities[55–57] and a somewhat similar effect resulting in lasing in vertices of a triangular valley-Hall laser with a controllable degree of asymmetry in the underlying periodic structure was reported in Ref. 58, our work is different in many aspects. We provide the illustration of topological corner lasers on a new platform—shallow waveguide arrays (as opposed to previous works on microrings or photonic crystal cavities with a 2D SSH configuration)—the idea that can be extended to polaritonic systems based on micropillar arrays, where nonlinear interactions of polaritons are repulsive[36,51,52] (in our case, nonlinearity is attractive). The continuous model, employed here, takes into account all features of the refractive index and gain landscapes, as opposed to simplified discrete models of HOTI lasers introduced before. We employ localized gain, which, when applied in different corners of our structure, offers a unique advantage of highly selective excitation of bulk, edge, or corner nonlinear topological states in HOTIs. The possibility of such selective excitation in our truly two-dimensional system is a nontrivial result by itself taking into account the complex spatial shape of the considered structure. We report on completely stable corner state lasing and bistability of the edge state lasing in higher-order topological insulators that can only be observed in the nonlinear medium. The detailed analysis of stability of lasing modes is provided for different values of linear gain and two-photon absorption coefficients. It is illustrated how lasing in corner states builds up from random noisy inputs. The stability of lasing in the presence of disorder is also illustrated.

Even when 0D corner states supported by our structure are strongly localized, they always penetrate into neighboring waveguides, where the field typically changes its sign. Importantly, by tuning the separation between waveguides, one can substantially change the area of the topological corner modes, which is not achievable, say, with single-element structures. The above-mentioned tunability of the corner mode area, in the case when lasing occurs in such a mode, may be used for the enhancement of the light–matter interactions and in the design of nonlinear photonic devices with better characteristics, as compared to usual topological lasers, where lasing is usually achieved in extended modes occupying the entire periphery of the structure. In addition, in corner lasers, the appearance of topological modes is guaranteed by simple deformation of the structure, allowing miniaturization and increasing performance in the nonlinear regime.

II. RESULTS AND DISCUSSION

A. Band structure and linear modes of the conservative system

The propagation dynamics of light beams in our dissipative system—the Kagome array of waveguides with tunable spacing—can be described by the nonlinear Schrödinger-like equation that in the dimensionless units reads as

$$i\frac{\partial\psi}{\partial z} = -\frac{1}{2}\left(\frac{\partial^2}{\partial x^2} + \frac{\partial^2}{\partial y^2}\right)\psi - (\mathcal{R}_{\mathrm{re}} - i\mathcal{R}_{\mathrm{im}} + i\gamma)\psi - (1 + i\alpha)|\psi|^2\psi. \quad (1)$$

Here, $\psi = (\kappa^2 w^2 n_{2,\mathrm{re}}/n_{\mathrm{re}})^{1/2}E$ is the dimensionless field amplitude; x, y are the transverse coordinates normalized to the characteristic scale w; z is the propagation distance scaled to the diffraction length κw^2; $\kappa = 2\pi n_{\mathrm{re}}/\lambda$ is the wavenumber; n_{re} and n_{im} ($n_{\mathrm{im}} \ll n_{\mathrm{re}}$) are the real and imaginary parts of the unperturbed linear refractive index of the material, respectively; $n_{2,\mathrm{re}}$ and $n_{2,\mathrm{im}}$ are the real and imaginary parts of the nonlinear refractive index, respectively; $\gamma = \kappa^2 w^2 n_{\mathrm{im}}/n_{\mathrm{re}}$ is the coefficient of linear losses that are assumed to be uniform; and $\alpha = n_{2,\mathrm{im}}/n_{2,\mathrm{re}}$ is the scaled coefficient characterizing nonlinear losses stemming from all sources, including intrinsic nonlinear losses of the medium and gain saturation in the first approximation. The refractive index distribution is described by the function $\mathcal{R}_{\mathrm{re}}(x,y) = p_{\mathrm{re}}\sum_{n,m}\mathcal{Q}(x - x_n, y - y_m)$ that is composed of Gaussian waveguides $\mathcal{Q} = \exp[-(x^2 + y^2)^3/d^6]$ with normalized depths of $p_{\mathrm{re}} = \kappa^2 w^2 \delta n_{\mathrm{re}}/n_{\mathrm{re}}$, where (x_n, y_m) are the coordinates of the sites of the Kagome lattice and $d = 0.5$ is the waveguide width. Here, we choose $p_{\mathrm{re}} = 10$ to make sure that every channel is a single-mode waveguide. For the definition of $\mathcal{R}_{\mathrm{im}}$, see Sec. II C.

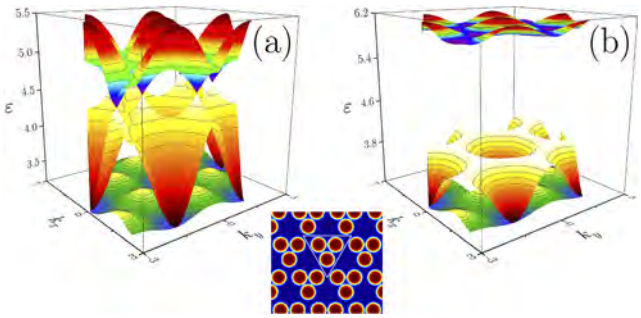

FIG. 1. First three bands for arrays with $r = 0.5a$ (a) and $r = 0.4a$ (b). The inset between panels shows the array profile at $r = 0.55a$. The white triangle illustrates the unit cell of the array.

Kagome waveguide arrays considered here can be deformed in a controllable fashion upon fabrication. The controllable deformation is described by the parameter r defining the shift of each second waveguide in the structure: see Fig. 1 for the band structure of the extended Kagome array and its profile with the unit cell indicated in the inset (also see the middle-left panel in Fig. 2, where the shift r and spacing $a = 2.5$ are indicated on the array profile shown with white contour lines). When $r = a/2$, one retrieves the standard Kagome array, and the band structure exhibits six Dirac cones between the upper two bands [Fig. 1(a)]. When $r < a/2$, the bandgap opens, as shown in Fig. 1(b).

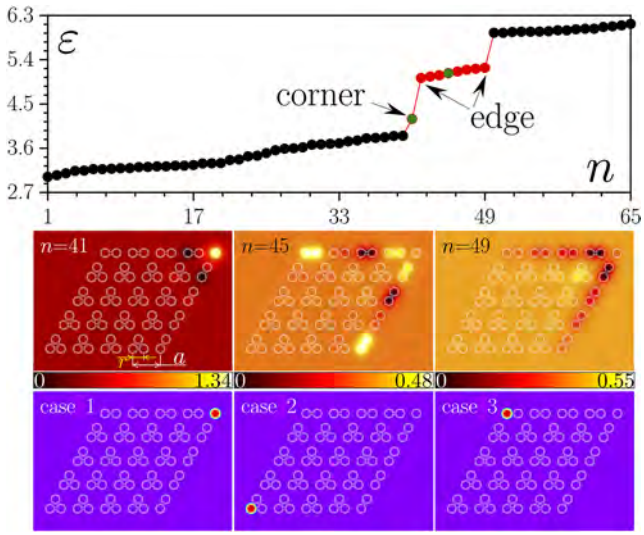

FIG. 2. Spectrum showing corner and edge states of the conservative system. (Top row) Linear spectrum $\varepsilon(n)$ of the array at $p_{\text{im}} = 0$, where n is the eigenvalue number. Color dots correspond to corner and edge states, while black dots correspond to bulk modes. Green dots indicate modes that lase first in the presence of localized gain acting in the top-right or top-left sites of the array. Middle row: Representative profiles of the corner and edge modes supported by the structure at $p_{\text{im}} = 0$. Array sites are indicated by white lines. Bottom row: Three different gain configurations that we consider, with the gain profile indicated by the red spot superimposed on the array profile.

We further truncate the infinite Kagome array such that a finite rhombic configuration forms (see white contours in panels of Fig. 2). The resulting system is essentially two-dimensional since it is obtained by truncation of the truly two-dimensional Kagome array and it is not equivalent to folded one-dimensional SSH chains. As we show below, our system possesses a unique spectrum of eigenmodes, where bulk, edge, and corner modes are present in an appropriate parameter range. Corner states in this truncated structure appear when the structure is topologically nontrivial at $r < a/2$. For the rhombic configuration in Fig. 2, they form in the top-right corner of the array. Due to the specific duality of our structure (that for the case of $r > a/2$ is equivalent to the structure with $r < a/2$ rotated by an angle of π), for the case with $r > a/2$, such states also emerge in the bottom-left corner. Notice that this duality is exclusively due to our choice of truncation of the structure (see below).

First, we consider the spectrum of the linear modes of our truncated array without gain and losses ($p_{\text{im}}, \gamma = 0$) and by omitting the last nonlinear term in Eq. (1). We find such modes from Eq. (1) in the form $\psi(x, y, z) = u(x, y)\exp(i\varepsilon z)$ by solving the resulting linear eigenvalue problem $\varepsilon u = (1/2)\left(\partial_x^2 + \partial_y^2\right)u + \mathcal{R}_{\text{re}}u$. For the array with $r = 0.4a$, the energies ε (propagation constants) of modes are shown in the top panel of Fig. 2. This spectrum includes one 0D corner state with eigenvalue number $n = 41$, a band of 1D edge states at $42 \le n \le 49$ shown by the red dots, and bulk modes (black dots). The structure of this spectrum remains qualitatively similar for larger arrays. In the middle row of Fig. 2, we show the real-valued amplitude distributions $u(x, y)$ for the conservative corner ($n = 41$) and edge states at $n = 45$ (green dot) and $n = 49$ (edge state with the largest ε value). Notice strong localization of light in the topological mode in the top-right corner of our continuous structure[14,15,22] for the selected r value. Even in this case, however, the mode penetrates into neighboring waveguides, where the field changes its sign. In fact, localization of corner modes strongly depends on the difference $r - a/2$, and such modes may extend far beyond the corner waveguide, when the above difference is small, demonstrating again the two-dimensional nature of our system. This possibility to control localization of topological corner modes will also be very important in the nonlinear lasing regime considered below, where by tuning $r - a/2$, one may control the area of the lasing mode, in contrast with the case of single waveguides, for example. Edge states that also appear in our system are characterized by excitations residing in the vicinity of two edges adjacent to the top-right corner, and they differ only by the number of nodes (where ψ vanishes) in the state along these edges.

In contrast to the rhombic configuration, the above-mentioned duality is absent in the triangular Kagome configuration obtained from the same infinite Kagome array (Fig. 3). Therefore, upon modifications of the parameter r controlling the shift of waveguides, topological corner states in the triangular structure emerge *only* in the regime, where $r < a/2$. To prove this, in Fig. 3(a), we show the spectrum of linear modes in the triangular configuration with $r = 0.4a$. The waveguide array with a triangular shape is shown in the inset. Due to the symmetry of the configuration, corner states simultaneously emerge in all three equivalent corners of the structure (green dots), and they have nearly identical propagation constants. Their field modulus distributions are shown in the panels below the spectrum. Notice that these corner states are linear, so an arbitrary linear superposition of such corner states also generates a correct corner

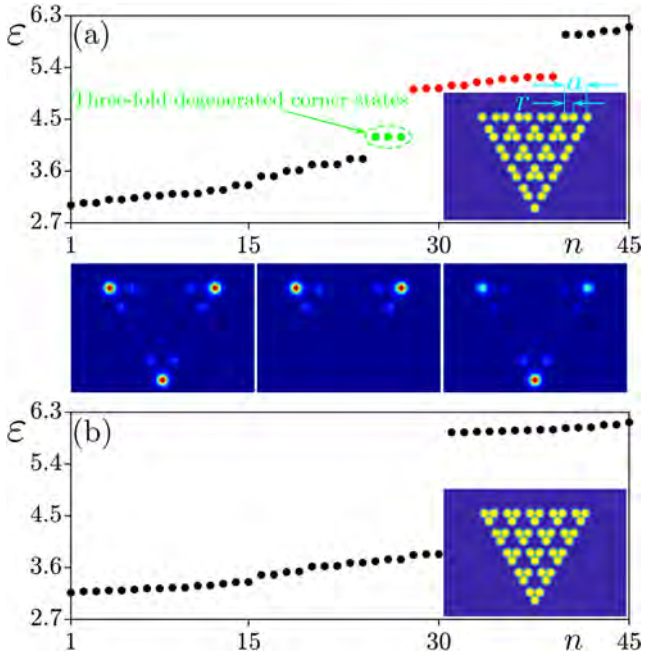

FIG. 3. Linear spectrum of modes in the triangular configuration. (a) $r = 0.4a$. Green dots are the corner states, red dots are the edge states, while black dots are the bulk states. The bottom panels show the three degenerated corner states. (b) $r = 0.6a$. There are only bulk states.

state of this system. The red dots in the spectrum correspond to the edge states localized on the sides of the triangle. To prove that in this structure, corner states emerge only at $r < a/2$, in Fig. 3(b), we show the linear spectrum of this triangular structure at $r = 0.6a$ (see also Fig. S7 in the supplementary material). There are no corner or edge states in the spectrum. This case is, therefore, topologically trivial. It should be stressed that the energies of corner states at $r < a/2$ in the triangular configuration are the same as the energy of the corner state in the rhombic configuration in Fig. 2. The only difference is that in the triangular configuration, corner states are triply degenerate and appear simultaneously in all three equivalent corners of the structure. Consequently, in the presence of gain and losses, lasing thresholds for corner states in rhombic and triangular configurations are also identical, as further discussed in the supplementary material. Since there is no degeneracy of corner states in the rhombic configuration, further throughout this paper, we adopt this structure for the analysis of the HOTI laser.

It should be mentioned that the topological properties of the Kagome array can be characterized by the bulk polarization that can be calculated using the formula $p_j = -S^{-1} \iint A_j d^2k$, where $A_j = -i\langle u|\partial k_j|u\rangle$ is the Berry connection and S is the area of the first Brillouin zone (BZ), with u being the Bloch mode of the structure. The details of calculation of the bulk polarization are presented in the supplementary material. The eigenvectors u can be calculated using the tight-binding Hamiltonian of the system. The system is in the topological phase when the polarization components are nonzero and in the trivial phase when the polarization is zero. The bulk polarizations (p'_x, p'_y) are calculated in the transformed coordinate system, where BZ is a square, with $(p'_x, p'_y) = (0,0)$ for $r > a/2$ (topologically trivial phase) and $(p'_x, p'_y) = (1/3, 1/3)$ for $r < a/2$ (topologically nontrivial phase). Thus, in our case, the appearance of corner states in the spectrum of the continuous system upon the variation of r was always correlated with the emergence of the nontrivial bulk polarization. Thus, further we consider a representative array with a rhombic configuration and $r = 0.4a$ illustrated in Fig. 2.

B. Linear modes of the dissipative system

To realize lasing, we provide localized gain in one of the corner sites of our rhombic structure (labeled case 1, case 2, and case 3, respectively, in the bottom row of Fig. 2). The inhomogeneous gain landscape is described in Eq. (1) by the function $\mathcal{R}_{\rm im}(x,y) = p_{im}\mathcal{Q}(x - x_c, y - y_c)$, where x_c, y_c are the coordinates of the corresponding corner waveguide, while the normalized gain amplitude is given by $p_{\rm im} = \kappa^2 w^2 \delta n_{\rm im}/n_{\rm re} (p_{\rm im} \ll p_{\rm re})$.

To understand how inhomogeneous gain and uniform losses affect linear modes of this structure, we calculate the spectrum of the system still neglecting the nonlinear effects but setting $\gamma = 0.05$ and increasing $p_{\rm im}$. The corresponding complex eigenvalue problem can be written as $\varepsilon u = (1/2)\left(\partial_x^2 + \partial_y^2\right)u + (\mathcal{R}_{\rm re} - i\mathcal{R}_{\rm im} + i\gamma)u$, where $\varepsilon = \varepsilon_{\rm re} + i\varepsilon_{\rm im}$, with $\varepsilon_{\rm re}$ and $\varepsilon_{\rm im}$ being the real and imaginary parts of eigenvalues, respectively. The sign of the imaginary part $\varepsilon_{\rm im}$ is determined by the losses γ and gain $\mathcal{R}_{\rm im}$. If $\varepsilon_{\rm im} < 0$, the modes are amplified, and if $\varepsilon_{\rm im} > 0$, they are damped. Figure 4 shows how $\varepsilon_{\rm re}$ and $\varepsilon_{\rm im}$ vary with the increase in the gain amplitude $p_{\rm im}$ for three different gain positions, corresponding to cases 1–3, outlined in Fig. 2. In Fig. 4, we plot the inverted value $-\varepsilon_{\rm im}$ for illustrative purposes. The positive values of $\varepsilon_{\rm im}$ shown by black dots and lying below the cyan plane ($\varepsilon_{\rm im} \equiv 0$) are, thus, associated with damped modes, while the negative $\varepsilon_{\rm im}$ values corresponding to the red dots lying above the cyan plane are associated with amplified states. Real parts $\varepsilon_{\rm re}$ are weakly affected by gain amplitude $p_{\rm im}$. One can see that in all three cases, growing modes appear when the gain amplitude $p_{\rm im}$ exceeds certain threshold, but there are important differences between these gain arrangements. For case 1, when gain is located in the corner supporting the topological corner state, only this state is amplified in the broad range of $p_{\rm im}$ values, while all other states are damped. Numerical simulations demonstrate that the lasing threshold for the topological corner state in case 1 takes the lowest possible value $p_{\rm im}^{\rm th} \sim 0.078$ for this structure. The lasing threshold remains the same in the triangular configuration (see the supplementary material). For case 2, only bulk states can lase above the highest lasing threshold $p_{\rm im}^{\rm th} \sim 0.255$. The number of such states increases with the increase in $p_{\rm im}$. In case 3, the edge state with $n = 45$ (whose counterpart in the conservative system is depicted in Fig. 2) lases first above the threshold $p_{\rm im}^{\rm th} \sim 0.225$, but a further increase in gain amplitude results in amplification of some of the bulk modes. The corner state is always damped in cases 2 and 3 in the interval of $p_{\rm im}$ values considered here, so one can expect to realize topological lasing only in case 1. This is natural taking into account that amplification efficiency is determined by the overlap of the corner mode with the gain landscape, which is the highest in the latter case, which also explains the lowest lasing threshold.

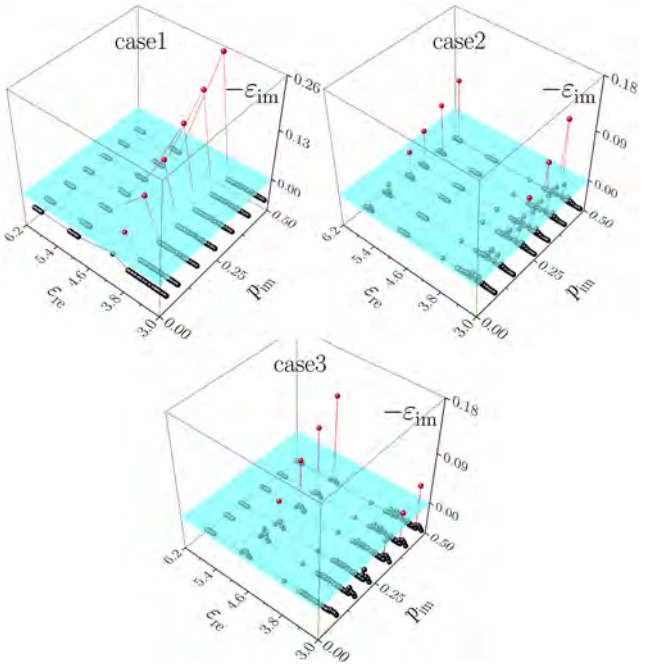

FIG. 4. Energy $\varepsilon = \varepsilon_{re} + i\varepsilon_{im}$ vs gain amplitude p_{im} for all modes of the system for three different locations of the channel with gain shown in Fig. 2. The real part ε_{re} of energy and its imaginary part $-\varepsilon_{im}$ with an inverted sign are shown simultaneously on two different axes since they may simultaneously change upon the variation of the gain amplitude p_{im}. For selected p_{im}, the projection of each dot on the $(\varepsilon_{re}, -\varepsilon_{im})$ plane gives the energy of the corresponding mode in the linear case. Only those modes that have $-\varepsilon_{im} > 0$ may lase. The dots corresponding to each lasing mode are shown in red, and they are located above the semi-transparent cyan plane corresponding to $\varepsilon_{im} = 0$. From this plot, one can see which modes from a given band start lasing first.

C. Families of nonlinear lasing modes

Amplification of the corner and edge states at $p_{im} > p_{im}^{th}$ can be eventually arrested by the nonlinear absorption. To explore the possibility of the exact and stable balance between diffraction, nonlinearity, gain, and absorption in this system, we now consider a complete model (1) with all nonlinear terms included and search for stationary nonlinear corner and edge states with constant power along the propagation distance. Their profiles are described by the following equation:

$$\varepsilon u = \frac{1}{2}\left(\frac{\partial^2}{\partial x^2} + \frac{\partial^2}{\partial y^2}\right)u + (\mathcal{R}_{re} - i\mathcal{R}_{im} + i\gamma)u + (1 + i\alpha)|u|^2 u, \quad (2)$$

with the real-valued nonlinear energy shift (or propagation constant) ε determined by the Kerr nonlinearity and two-photon absorption. On physical grounds, stabilization of the lasing modes is achieved due to two-photon absorption that prevents the amplitude from unlimited growth above the lasing threshold. Nonlinear absorption counteracts the tendency for self-localization due to self-focusing nonlinearity; it leads to the appearance of nontrivial internal currents in nonlinear solution, which are directed outward the pump spot, and results in spatial broadening of stable lasing states for larger values of the α coefficient. Since ε is not an independent parameter in this dissipative system, we use the Newton method complemented by the power balance condition to obtain families of the nonlinear lasing states parameterized by the gain amplitude p_{im}, which can be written as follows:

$$\iint \left[(\mathcal{R}_{im} - \gamma)|\psi|^2 - \alpha|\psi|^4\right]dxdy = 0. \quad (3)$$

Notice that standard simulation of evolution does not provide unstable branches because in such a method, the wave converges only to dynamically stable attractors. In contrast, our method, based on the simultaneous solution of Eqs. (2) and (3), allows us to get all solutions, which may be stable or unstable, and even determine bistable regimes.

To characterize nonlinear families of the corner and edge states (emerging in cases 1 and 3, respectively) in our system, we plot their peak amplitude $|\psi|_{max}$ and nonlinear energy shifts ε as functions of p_{im} in the left panels of Figs. 5(a) and 5(b), respectively, for different nonlinear absorption coefficients α. The corresponding gain landscapes are also presented for each case. In both cases, stationary nonlinear modes appear when the gain amplitude p_{im} exceeds the corresponding lasing threshold (for example, in case 1 it is $p_{im}^{th} \sim 0.078$). These states are characterized by complex internal currents, but for them, nonlinear absorption exactly integrally compensates inhomogeneous gain. The nonlinear energy shift ε increases almost linearly with p_{im} in the region $p_{im} > p_{im}^{th}$ (all modes are damped in the region

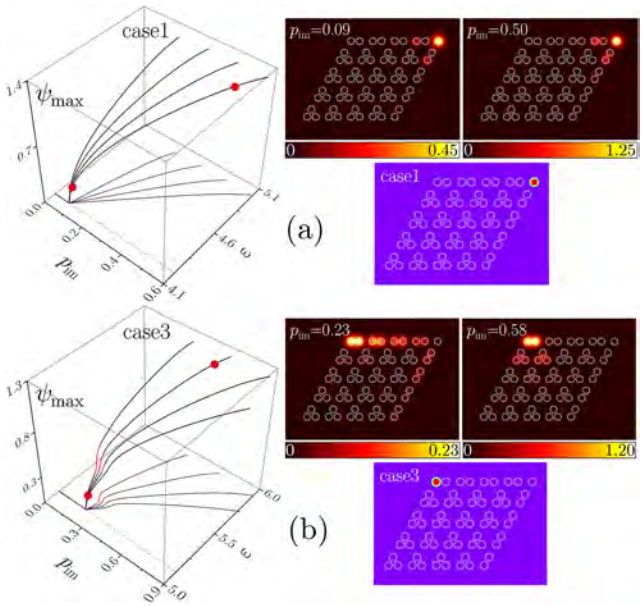

FIG. 5. Nonlinear lasing state families: maximal amplitude ψ_{max} and propagation constant ε of the nonlinear lasing mode vs gain amplitude p_{im} for two different locations of the amplifying channel [(a) case 1 and (b) case 3] and nonlinear absorption coefficients $\alpha = 0.1$, 0.2, 0.3, and 0.4 (in all plots, the left outermost curve corresponds to $\alpha = 0.1$, while the right one to $\alpha = 0.4$). Stable branches are shown in black, and unstable branches are shown in red. Red dots correspond to $|\psi(x, y)|$ distributions shown in the top row. The bottom row schematically shows the channel with gain in the array.

$p_{im} < p_{im}^{th}$). At $p_{im} = p_{im}^{th}$, it naturally coincides with the real part of the eigenvalue ε_{re} of the linear edge state from which the nonlinear mode bifurcates [as shown by the bottom dotted line in the (p_{im}, ε) plane in Fig. 5(a)], allowing us to uniquely identify the state giving rise to the stable lasing mode. Thus, such nonlinear corner states are of topological origin since they bifurcate from 0D linear topological corner modes.[1,14,15,22] Since we only consider corner lasing modes forming in the gap, which do not couple to edge or bulk modes, we show in Fig. 5(a) the curves for ε values below the band occupied by the eigenvalues of the linear edge states (i.e., below red dots in the spectrum of Fig. 2). In the top two panels in the right column in Fig. 5(a), we show $|\psi|$ distributions for corner lasing states at $\alpha = 0.4$ for different gain amplitudes, corresponding to the red dots, one close to lasing threshold ($p_{im} = 0.09$) and the other rather far from it ($p_{im} = 0.50$). One can see that for $r = 0.4a$, such states are very well localized and that most of their energy is concentrated in the top-right corner site. However, when $r \to a/2$, lasing can be achieved even in weakly localized corner modes, confirming the tunability of this system mentioned in the introduction. Quantitatively similar results are also obtained in the triangular configuration, as shown in the supplementary material.

In contrast, when gain is provided in the top-left corner of the array, which corresponds to case 3 [see the bottom panels in the right column of Fig. 5(b)], the conditions for the most efficient amplification are met for the edge state with $n = 45$ (upper green dot in Fig. 2), which starts lasing when the gain amplitude exceeds threshold $p_{im}^{th} \sim 0.225$ that, nevertheless, is substantially larger than the threshold obtained for the corner state in case 1. Still, it is remarkable that by choosing the gain location in this system, one can selectively excite either 0D corner or 1D edge states. This illustrates a rich variety of lasing regimes that can be observed in our structure, which would not be available in single-waveguide geometries, for example. Nonlinear families corresponding to different absorption coefficients for case 3 are displayed in the left panel of Fig. 5(b). The nonlinear lasing edge state bifurcates from the linear edge state with $n = 45$, and its energy grows with p_{im} until it reaches the gap edge, above which coupling with bulk modes occurs. Interestingly, despite the fact that usual linear amplification is used, rather than pump with certain energy, the bistability domain is encountered for edge states in case 3, where three solutions can coexist for the same p_{im} value. The encountered bistability offers the unique advantage to achieve lasing in the edge states with different internal structures and amplitudes for certain p_{im} values. $|\psi|$ distributions from the middle branch of $\varepsilon(p_{im})$ dependence clearly show strong coupling with the opposite edge of the rhombic structure. In the top panels in the right column of Fig. 5(b), we illustrate representative $|\psi|$ distributions from the lower and upper branches corresponding to the red dots at $p_{im} = 0.23$ and $p_{im} = 0.58$. With increasing gain amplitude p_{im}, the nonlinear edge state that was initially strongly extended over two edges of the rhombus, gradually contracts toward the top-left corner of the structure. Therefore, the profile of the nonlinear edge lasing state at sufficiently high p_{im} may strongly differ from its linear counterpart shown in the middle panel in the second row ($n = 45$) in Fig. 2. From the dependencies shown in Fig. 5, one can see that for a fixed gain amplitude p_{im}, the peak amplitude of the nonlinear lasing state decreases with the increase in the nonlinear absorption coefficient α. The energy interval, where nonlinear states exist, increases with the increase in the nonlinear absorption.

On physical grounds, one can perform comparison of lasing in corner states of the Kagome array and in the isolated waveguide. While there is no fundamental difference in lasing efficiency, the Kagome array provides tunability that is absent for single waveguides since the structure of the lasing mode in the Kagome array strongly depends on the dimerization parameter r. The field of corner lasing modes is localized mostly on one of the sublattices, forming the Kagome array, and it changes its sign between unit cells, which results in staggered tails, as it is obvious from the profile of the corner mode ($n = 41$) from Fig. 2. Thus, the presence of the array does allow us to control the spatial extent of the lasing pattern and is, therefore, very important (thus, at r values close to $a/2$, lasing will occur in the mode strongly penetrating into the depth of the array, even though gain is provided only in one waveguide). A detailed comparison between lasing in the Kagome array and in the isolated waveguide is presented in the supplementary material.

The stability of the nonlinear lasing modes is central from the point of view of construction of topological lasers because it guarantees that the only one spatial mode will be excited and there will be no oscillations due to instabilities or beatings between several excited modes. Stability analysis for nonlinear lasing modes obtained with the Newton method was performed by adding into their profiles small-amplitude noise (typically up to 2% in amplitude) and propagating them (by using the split-step Fourier method) over large distances, $z \sim 10^4$, far exceeding the length of any realistic sample. In all cases, the amplitude of modes, which are stable, was returning to the unperturbed value, and such modes maintained their internal structure. This method allows us capturing even weak instabilities and accurately determining stability domains. The regions where lasing is stable or unstable are identified in Fig. 5, where black curves correspond to stable lasing states, while red ones to unstable states. We found that corner lasing states in case 1 are always stable, even for low nonlinear absorption coefficients [Fig. 5(a)]. Nonlinear edge states in case 3 can also be stable, but the middle branches in the encountered bistability regions are always unstable. The bistability illustrated in Fig. 5(b) is a result of nonlinear competition between several coexisting edge states that all experience amplification. Indeed, we have found that the structure of the lasing state substantially changes in the red unstable region in Fig. 5(b) with the increase in its peak amplitude, i.e., at low and high peak amplitudes, the relative weights of different edge states in lasing modes change because they experience different gains (the overlap of their spatial profiles with the pump spot is different) and at the same time the relative weights of modes determine total absorption experienced by the wave. Due to this competition, several stationary nonlinear configurations can coexist for the same gain amplitude, giving rise to bistability. The unstable regions gradually disappear with the increase in the nonlinear absorption, until the entire branch of the edge states becomes stable [Fig. 5(b)].

D. Noise-stimulated lasing

It is interesting to mention that lasing states in this dissipative system, being stable attractors, can be excited from the broad range of the initial conditions. For instance, they emerge from broadband random noise that initially excites all modes of the system, upon subsequent nonlinear competition between these modes, some of which exhibit preferential amplification. This once again confirms

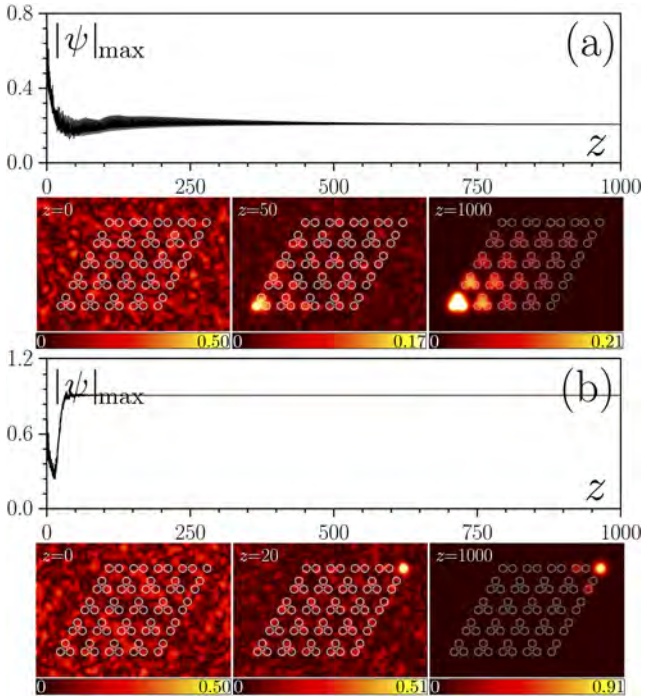

FIG. 6. Lasing states excited by noisy inputs. Excitation dynamics of nonlinear lasing modes at $p_{im} = 0.3$ and $\alpha = 0.4$ in case 2, when gain is provided in the corner, which does not support the topological state (a), and case 1, when gain acts in the corner where the topological mode resides (b), from noisy inputs. In each case, the dependence of peak amplitude $|\psi|_{max}$ on the distance is shown together with $|\psi|$ distributions at selected propagation distances.

the robustness of the nonlinear lasing states. In order to illustrate this type of laser operation, in Fig. 6, we show different stages of the evolution dynamics of noisy input excitations for gain landscapes corresponding to cases 1 and 2. Figure 6(a) shows the peak amplitude $|\psi|_{max}$ of the field vs propagation distance z for case 2. One can see that the peak amplitude $|\psi|_{max}$ exhibits long gradually decaying oscillations approaching the stationary value only after a long propagation distance, $z \sim 750$. The corresponding $|\psi|$ distributions reveal transition from noisy input to a regular but extremely extended pattern that occupies practically the entire waveguide array. Even though this pattern features somewhat larger amplitude in the bottom-left corner due to high localization of the gain profile, it clearly indicates the excitation of the bulk modes of the structure in accordance with the spectrum of Fig. 4 (increasing the size of the waveguide array leads to further expansion of this pattern). In contrast, for the gain landscape corresponding to case 1, the peak amplitude of the excitation quickly reaches (at the distance $z \sim 100$) its asymptotic value, as illustrated in Fig. 6(b). The nonlinear mode quickly concentrates in the top-right corner, supporting the topological corner state, and then remains strongly localized and stable at all propagation distances.

E. Discussion

Propagation of light in shallow waveguide arrays adopted in this work is perfectly described within the frames of the paraxial approximation, assuming excitation at a single frequency, where appropriate spatially inhomogeneous gain can be realized with existing techniques. Nonlinear dissipative states emerging in such arrays are the result of competition between different spatial modes of the system, some of which are preferentially amplified, but all nonlinear dissipative states reported here can be traced back to the linear modes of the structure from which they emerge at threshold gain amplitude $p_{im} = p_{im}^{th}$, the fact that allows us to claim single spatial mode lasing in this system. The competition between modes occurs due to conservative and dissipative parts of nonlinearity present in Eq. (1), which determines also the dynamical stability of the emerging states. The results reported here can be extended to other optical or optoelectronic systems, such as photonic crystals, photonic crystal fibers, and structured polariton microcavities, where spatially inhomogeneous gain and suitable refractive index/potential energy landscapes can be fabricated or induced optically.

The system based on the waveguide arrays suggested in this work can be practically implemented with doped (for example, with Er) chalcogenide glasses (such as GaLaS or AsSe), where waveguide arrays can be written with tightly focused laser pulses. The nonlinear coefficient in such materials is about $n_{2,re} \sim 1 \times 10^{-17}$ m^2/W, while the nonlinear absorption coefficient varies between $n_{2,im} \sim 10^{-19}$ and 10^{-17} m^2/W depending on the composition of the glass.[59–61] In this case, one finds that when transverse coordinates are scaled to 10 μm, the dimensionless propagation distance in Eq. (1) is scaled to the diffraction length of ~ 1.5 mm; the waveguide depth of $p_{re} = 10$ corresponds to real refractive index contrast $\sim 1.13 \times 10^{-3}$, while the gain amplitude $p_{im} = 0.1$ corresponds to $\delta n_{im} \sim 1 \times 10^{-5}$ for the unperturbed refractive index $n_{re} \sim 2.81$ at the wavelength $\lambda = 1.08\,\mu$m. The structure proposed here can also be implemented in planar pumped photonic crystal structures.[42,62]

It should be stressed that the structure considered here allows for considerable size of the topological gap, the property that is important for applications.[63] According to the spectrum presented in Fig. 2, one finds that for $r = 0.4a$, the bandgap opening in the spectrum constitutes up to 42.8% according to ratio = $(\varepsilon_{top} - \varepsilon_{bottom})/\varepsilon_{middle}$, where ε_{top}, ε_{middle}, and ε_{bottom} correspond to the top edge, middle, and bottom edge of the bandgap. Considering that there are both corner and edge states in the bandgap, the width of the gap (where the corner state is located) between the edge states and top of the bulk band is about 26.51% of the whole bandwidth. We believe that the ratio can be improved if the value of r is decreased below $0.4a$. However, there are some limitations because for too small values of r, the neighboring sites in the array may start fusing. Large size of the topological gap is beneficial for topological protection of the lasing regime.

The important property of topological lasers is that lasing in this structure remains stable as long as variations of eigenvalues of the modes that it supports due to inevitable disorder upon fabrication of the structure do not lead to closure of the gap so that corner modes persist and experience the largest gain, when pump is provided in the corner waveguide. In the supplementary material, we introduce various types of perturbations (most of them break the spatial symmetry of the system[64]) into the Kagome array, including random variations of waveguide depths/positions in the bulk, at the edge, or only in the corner sites. For all these types of perturbations, the robustness of the corner state was confirmed.

The conclusion is that when disorder is provided in depths of the bulk and edge waveguides of the array but not in the corner ones, the gap and corner mode residing in the gap persist even for 10% perturbations. When disorder is present also in the corner waveguide, its impact on corner modes is stronger and may lead to the shift of the eigenvalue of the corner mode, but for moderate disorder amplitudes, corner states also persist in the gap and do not couple to bulk modes. It should be stressed that for the latter type of disorder, the energies of the corner states start overlapping with the continuous band only when the actual strength of disorder $\delta \cdot p_{re}$ [here, we introduce disorder by changing the depth of the waveguide with indices n, m to $p_{re}(1 + \delta_{n,m})$, where $\delta_{n,m}$ is a random number uniformly distributed within the interval $[-\delta, +\delta]$] is comparable with the width of the topological gap, i.e., when disorder is not small. Shifting the top-right corner site of the structure along the direction parallel/orthogonal to the line connecting the top-right and bottom-left corners of rhombus also does not lead to destruction of the corner state and demonstrates its robustness. A table that illustrates all the above-mentioned perturbations, examples of the corresponding robust corner states, and spectra of all modes of the system (illustrating that no new modes appeared in the gap) can be found in the supplementary material. Even in the presence of disorder, when localized gain is provided in the corner channel, corner modes do lase above the lowest threshold, so in this sense, the robustness of lasing operation with respect to disorder is obvious. It should be mentioned that typical uncertainties in the fabrication process of the structure strongly depend on the particular technology, for example, for direct laser writing of waveguides, they usually do not exceed 2%.[65]

To support the claim of more robust behavior of the topological system, we also compare the behavior of the same platform in topological and nontopological regimes. Thus, in the supplementary material, we show the spectrum of the trivial array (i.e., the array with $r = a/2$) and examples of the corresponding modes that are all delocalized. We found that when gain is provided in the corner of the trivial Kagome array with $r = a/2$, the threshold for lasing is substantially higher than that in the topological phase, at $r = 0.4a$. The family of nonlinear lasing modes now bifurcates from one of the delocalized linear modes since there is no gap in the spectrum. Due to nonlinear competition of several bulk modes, they may mix in the lasing state. This is manifested in the change of the slope of the dependence of the maximal wave amplitude and nonlinear energy shift on the gain parameter.

There is an ongoing debate on topological characterization of modes in Kagome arrays[66,67] with many evidences of topological behavior of this system reported experimentally. The emergence of corner modes in the spectrum of our continuous system (that automatically takes into account long-range coupling) was always correlated with the appearance of nontrivial bulk polarization calculated in the frames of the simplified discrete model. While this may not be the case for multilayer topological systems, here we would like to emphasize that the Kagome array under the action of perturbations behaves very similar to the well-established topological Su–Schrieffer–Heeger (SSH) model, and at the same time, it remains a truly two-dimensional system. The comparison of the robustness of corner modes of the Kagome array and topological modes of the SSH model under the action of different perturbations can be found in the supplementary material. We find that in both models, energies of the topological corner states may shift into the band but only when perturbations are added into the corner (or the edge in the case of SSH chains) site and when their amplitude is comparable with the width of the whole topological gap. As confirmed by the calculation of bulk polarization, this supports the conclusion about topological nature of corner states in the Kagome array.

III. CONCLUSIONS

In summary, we have proposed corner state lasers based on Kagome waveguide arrays with a rhombic configuration. Stable corner lasing states with low threshold bifurcate from the topological corner modes under the balance between diffraction, focusing nonlinearity, uniform loss, two-photon absorption, and gain provided in the selected corner of the structure, supporting topological states. Applying gain in the other corners of the array allows us achieving lasing in edge states or bulk modes but above much higher lasing thresholds. Excitation of topological and nontopological nonlinear modes from noisy inputs is also illustrated, and it is found that formation of nontopological modes requires much longer propagation distances, and they appear to be weakly localized, in contrast to strongly localized nonlinear corner lasing modes. This work paves the way for realization of 0D topological corner lasers based on HOTIs and may inspire research of topological transitions in similar dissipative systems.

SUPPLEMENTARY MATERIAL

See the supplementary material for the details about the bulk polarizations, robustness analysis on the corner state, and other issues mentioned in the main text.

ACKNOWLEDGMENTS

This work was supported by the National Natural Science Foundation of China (Grant Nos. 12074308 and U1537210), the Russian Science Foundation (Grant No. 21-12-00096), and the Fundamental Research Funds for the Central Universities (Grant Nos. xzy012019038 and xzy022019076). H.Z. and Y.Z. acknowledge the computational resources provided by the HPC platform of Xi'an Jiaotong University.

DATA AVAILABILITY

The data that support the findings of this study are available from the corresponding author upon reasonable request.

REFERENCES

[1] M. Ezawa, "Higher-order topological insulators and semimetals on the breathing Kagome and pyrochlore lattices," Phys. Rev. Lett. **120**, 026801 (2018).
[2] L. Trifunovic and P. W. Brouwer, "Higher-order bulk-boundary correspondence for topological crystalline phases," Phys. Rev. X **9**, 011012 (2019).
[3] W. A. Benalcazar, B. A. Bernevig, and T. L. Hughes, "Quantized electric multipole insulators," Science **357**, 61–66 (2017).
[4] J. Langbehn, Y. Peng, L. Trifunovic, F. Von Oppen, and P. W. Brouwer, "Reflection-symmetric second-order topological insulators and superconductors," Phys. Rev. Lett. **119**, 246401 (2017).

[5]Z. Song, Z. Fang, and C. Fang, "(d − 2)-dimensional edge states of rotation symmetry protected topological states," Phys. Rev. Lett. **119**, 246402 (2017).
[6]F. Schindler, A. M. Cook, M. G. Vergniory, Z. Wang, S. S. P. Parkin, B. A. Bernevig, and T. Neupert, "Higher-order topological insulators," Sci. Adv. **4**, eaat0346 (2018).
[7]M. J. Park, Y. Kim, G. Y. Cho, and S. Lee, "Higher-order topological insulator in twisted bilayer graphene," Phys. Rev. Lett. **123**, 216803 (2019).
[8]Z. Yan, F. Song, and Z. Wang, "Majorana corner modes in a high-temperature platform," Phys. Rev. Lett. **121**, 096803 (2018).
[9]Q. Wang, C.-C. Liu, Y.-M. Lu, and F. Zhang, "High-temperature Majorana corner states," Phys. Rev. Lett. **121**, 186801 (2018).
[10]C.-H. Hsu, P. Stano, J. Klinovaja, and D. Loss, "Majorana Kramers pairs in higher-order topological insulators," Phys. Rev. Lett. **121**, 196801 (2018).
[11]S. Imhof, C. Berger, F. Bayer, J. Brehm, L. W. Molenkamp, T. Kiessling, F. Schindler, C. H. Lee, M. Greiter, T. Neupert, and R. Thomale, "Topolectrical-circuit realization of topological corner modes," Nat. Phys. **14**, 925–929 (2018).
[12]M. Serra-Garcia, V. Peri, R. Süsstrunk, O. R. Bilal, T. Larsen, L. G. Villanueva, and S. D. Huber, "Observation of a phononic quadrupole topological insulator," Nature **555**, 342–345 (2018).
[13]H. Fan, B. Xia, L. Tong, S. Zheng, and D. Yu, "Elastic higher-order topological insulator with topologically protected corner states," Phys. Rev. Lett. **122**, 204301 (2019).
[14]H. Xue, Y. Yang, F. Gao, Y. Chong, and B. Zhang, "Acoustic higher-order topological insulator on a Kagome lattice," Nat. Mater. **18**, 108–112 (2019).
[15]X. Ni, M. Weiner, A. Alù, and A. B. Khanikaev, "Observation of higher-order topological acoustic states protected by generalized chiral symmetry," Nat. Mater. **18**, 113–120 (2019).
[16]X. Zhang, H.-X. Wang, Z.-K. Lin, Y. Tian, B. Xie, M.-H. Lu, Y.-F. Chen, and J.-H. Jiang, "Second-order topology and multidimensional topological transitions in sonic crystals," Nat. Phys. **15**, 582–588 (2019).
[17]X. Zhang, B.-Y. Xie, H.-F. Wang, X. Xu, Y. Tian, J.-H. Jiang, M.-H. Lu, and Y.-F. Chen, "Dimensional hierarchy of higher-order topology in three-dimensional sonic crystals," Nat. Commun. **10**, 5331 (2019).
[18]C. W. Peterson, W. A. Benalcazar, T. L. Hughes, and G. Bahl, "A quantized microwave quadrupole insulator with topologically protected corner states," Nature **555**, 346–350 (2018).
[19]J. Noh, W. A. Benalcazar, S. Huang, M. J. Collins, K. P. Chen, T. L. Hughes, and M. C. Rechtsman, "Topological protection of photonic mid-gap defect modes," Nat. Photonics **12**, 408–415 (2018).
[20]B.-Y. Xie, H.-F. Wang, H.-X. Wang, X.-Y. Zhu, J.-H. Jiang, M.-H. Lu, and Y.-F. Chen, "Second-order photonic topological insulator with corner states," Phys. Rev. B **98**, 205147 (2018).
[21]F.-F. Li, H.-X. Wang, Z. Xiong, Q. Lou, P. Chen, R.-X. Wu, Y. Poo, J.-H. Jiang, and S. John, "Topological light-trapping on a dislocation," Nat. Commun. **9**, 2462 (2018).
[22]A. El Hassan, F. K. Kunst, A. Moritz, G. Andler, E. J. Bergholtz, and M. Bourennane, "Corner states of light in photonic waveguides," Nat. Photonics **13**, 697–700 (2019).
[23]S. Mittal, V. V. Orre, G. Zhu, M. A. Gorlach, A. Poddubny, and M. Hafezi, "Photonic quadrupole topological phases," Nat. Photonics **13**, 692–696 (2019).
[24]X.-D. Chen, W.-M. Deng, F.-L. Shi, F.-L. Zhao, M. Chen, and J.-W. Dong, "Direct observation of corner states in second-order topological photonic crystal slabs," Phys. Rev. Lett. **122**, 233902 (2019).
[25]B.-Y. Xie, G.-X. Su, H.-F. Wang, H. Su, X.-P. Shen, P. Zhan, M.-H. Lu, Z.-L. Wang, and Y.-F. Chen, "Visualization of higher-order topological insulating phases in two-dimensional dielectric photonic crystals," Phys. Rev. Lett. **122**, 233903 (2019).
[26]Y. Ota, F. Liu, R. Katsumi, K. Watanabe, K. Wakabayashi, Y. Arakawa, and S. Iwamoto, "Photonic crystal nanocavity based on a topological corner state," Optica **6**, 786–789 (2019).
[27]L. Lu, J. D. Joannopoulos, and M. Soljačić, "Topological photonics," Nat. Photonics **8**, 821–829 (2014).
[28]T. Ozawa, H. M. Price, A. Amo, N. Goldman, M. Hafezi, L. Lu, M. C. Rechtsman, D. Schuster, J. Simon, O. Zilberberg, and I. Carusotto, "Topological photonics," Rev. Mod. Phys. **91**, 015006 (2019).
[29]X.-W. Luo and C. Zhang, "Higher-order topological corner states induced by gain and loss," Phys. Rev. Lett. **123**, 073601 (2019).
[30]T. Liu, Y.-R. Zhang, Q. Ai, Z. Gong, K. Kawabata, M. Ueda, and F. Nori, "Second-order topological phases in non-Hermitian systems," Phys. Rev. Lett. **122**, 076801 (2019).
[31]Z. Zhang, M. R. López, Y. Cheng, X. Liu, and J. Christensen, "Non-Hermitian sonic second-order topological insulator," Phys. Rev. Lett. **122**, 195501 (2019).
[32]A. Yoshida, Y. Otaki, R. Otaki, and T. Fukui, "Edge states, corner states, and flat bands in a two-dimensional PT-symmetric system," Phys. Rev. B **100**, 125125 (2019).
[33]F. Zangeneh-Nejad and R. Fleury, "Nonlinear second-order topological insulators," Phys. Rev. Lett. **123**, 053902 (2019).
[34]R. Banerjee, S. Mandal, and T. C. H. Liew, "Coupling between exciton-polariton corner modes through edge states," Phys. Rev. Lett. **124**, 063901 (2020).
[35]L. Pilozzi and C. Conti, "Topological lasing in resonant photonic structures," Phys. Rev. B **93**, 195317 (2016).
[36]P. St-Jean, V. Goblot, E. Galopin, A. Lemaître, T. Ozawa, L. Le Gratiet, I. Sagnes, J. Bloch, and A. Amo, "Lasing in topological edge states of a one-dimensional lattice," Nat. Photonics **11**, 651–656 (2017).
[37]M. Parto, S. Wittek, H. Hodaei, G. Harari, M. A. Bandres, J. Ren, M. C. Rechtsman, M. Segev, D. N. Christodoulides, and M. Khajavikhan, "Edge-mode lasing in 1D topological active arrays," Phys. Rev. Lett. **120**, 113901 (2018).
[38]H. Zhao, P. Miao, M. H. Teimourpour, S. Malzard, R. El-Ganainy, H. Schomerus, and L. Feng, "Topological hybrid silicon microlasers," Nat. Commun. **9**, 981 (2018).
[39]S. Longhi, Y. Kominis, and V. Kovanis, "Presence of temporal dynamical instabilities in topological insulator lasers," Europhys. Lett. **122**, 14004 (2018).
[40]S. Malzard and H. Schomerus, "Nonlinear mode competition and symmetry-protected power oscillations in topological lasers," New J. Phys. **20**, 063044 (2018).
[41]D. Smirnova, D. Leykam, Y. Chong, and Y. Kivshar, "Nonlinear topological photonics," Appl. Phys. Rev. **7**, 021306 (2020).
[42]B. Bahari, A. Ndao, F. Vallini, A. El Amili, Y. Fainman, and B. Kanté, "Nonreciprocal lasing in topological cavities of arbitrary geometries," Science **358**, 636–639 (2017).
[43]G. Harari, M. A. Bandres, Y. Lumer, M. C. Rechtsman, Y. D. Chong, M. Khajavikhan, D. N. Christodoulides, and M. Segev, "Topological insulator laser: Theory," Science **359**, eaar4003 (2018).
[44]M. A. Bandres, S. Wittek, G. Harari, M. Parto, J. Ren, M. Segev, D. N. Christodoulides, and M. Khajavikhan, "Topological insulator laser: Experiments," Science **359**, eaar4005 (2018).
[45]Y. Zeng, U. Chattopadhyay, B. Zhu, B. Qiang, J. Li, Y. Jin, L. Li, A. G. Davies, E. H. Linfield, B. Zhang, Y. Chong, and Q. J. Wang, "Electrically pumped topological laser with valley edge modes," Nature **578**, 246–250 (2020).
[46]H. Zhong, Y. Li, D. Song, Y. V. Kartashov, Y. Q. Zhang, Y. P. Zhang, and Z. Chen, "Topological valley Hall edge state lasing," Laser Photonics Rev. **14**, 2000001 (2020).
[47]Y. Gong, S. Wong, A. J. Bennett, D. L. Huffaker, and S. S. Oh, "Topological insulator laser using valley-Hall photonic crystals," ACS Photonics **7**, 2089–2097 (2020).
[48]D. Smirnova, A. Tripathi, S. Kruk, M.-S. Hwang, H.-R. Kim, H.-G. Park, and Y. Kivshar, "Room-temperature lasing from nanophotonic topological cavities," Light: Sci. Appl. **9**, 127 (2020).
[49]S. K. Ivanov, Y. Zhang, Y. V. Kartashov, and D. V. Skryabin, "Floquet topological insulator laser," APL Photonics **4**, 126101 (2019).
[50]M. Seclì, M. Capone, and I. Carusotto, "Theory of chiral edge state lasing in a two-dimensional topological system," Phys. Rev. Res. **1**, 033148 (2018).
[51]S. Klembt, T. H. Harder, O. A. Egorov, K. Winkler, R. Ge, M. A. Bandres, M. Emmerling, L. Worschech, T. C. H. Liew, M. Segev, C. Schneider, and S. Höfling, "Exciton-polariton topological insulator," Nature **562**, 552–556 (2018).
[52]Y. V. Kartashov and D. V. Skryabin, "Two-dimensional topological polariton laser," Phys. Rev. Lett. **122**, 083902 (2019).

[53]W. Zhang, X. Chen, Y. V. Kartashov, D. V. Skryabin, and F. Ye, "Finite-dimensional bistable topological insulators: From small to large," Laser Photonics Rev. **13**, 1900198 (2019).
[54]M. Li, D. Zhirihin, M. Gorlach, X. Ni, D. Filonov, A. Slobozhanyuk, A. Alù, and A. B. Khanikaev, "Higher-order topological states in photonic Kagome crystals with long-range interactions," Nat. Photonics **14**, 89–94 (2020).
[55]W. X. Zhang, X. Xie, H. M. Hao, J. Dang, S. Xiao, S. Shi, H. Ni, Z. Niu, C. Wang, K. Jin, X. Zhang, and X. Xu, "Low-threshold topological nanolasers based on second-order corner state," Light: Sci. Appl. **9**, 109 (2020).
[56]C. Han, M. Kang, and H. Jeon, "Lasing at multidimensional topological states in a two-dimensional photonic crystal structure," ACS Photonics **7**, 2027–2036 (2020).
[57]H.-R. Kim, M.-S. Hwang, D. Smirnova, K.-Y. Jeong, Y. Kivshar, and H.-G. Park, "Multipolar lasing modes from topological corner states," Nat. Commun. **11**, 5758 (2020).
[58]W. Noh, H. Nasari, H.-M. Kim, Q. Le-Van, Z. Jia, C.-H. Huang, and B. Kanté, "Experimental demonstration of single-mode topological valley-Hall lasing at telecommunication wavelength controlled by the degree of asymmetry," Opt. Lett. **45**, 4108–4111 (2020).
[59]A. Zakery and S. R. Elliott, *Optical Nonlinearities in Chalcogenide Glasses and Their Applications* (Springer, Berlin, Heidelberg, 2007).
[60]F. Smektala, C. Quemard, V. Couderc, and A. Barthélémy, "Non-linear optical properties of chalcogenide glasses measured by Z-scan," J. Non-Cryst. Solids **274**, 232–237 (2000).
[61]J. Harrington, *Infrared Fibers and Their Applications* (SPIE Press, Bellingham, WA, 2003).
[62]Z.-K. Shao, H.-Z. Chen, S. Wang, X.-R. Mao, Z.-Q. Yang, S.-L. Wang, X.-X. Wang, X. Hu, and R.-M. Ma, "A high-performance topological bulk laser based on band-inversion-induced reflection," Nat. Nanotechnol. **15**, 67–72 (2020).
[63]L. Zhang, Y. Yang, Z.-K. Lin, P. Qin, Q. Chen, F. Gao, E. Li, J.-H. Jiang, B. Zhang, and H. Chen, "Higher-order topological states in surface-wave photonic crystals," Adv. Sci. **7**, 1902724 (2020).
[64]M. Proctor, P. A. Huidobro, B. Bradlyn, M. B. de Paz, M. G. Vergniory, D. Bercioux, and A. García-Etxarri, "On the robustness of topological corner modes in photonic crystals," Phys. Rev. Res. **2**, 042038 (2020).
[65]A. Szameit and S. Nolte, "Discrete optics in femtosecond-laser-written photonic structures," J. Phys. B: At., Mol. Opt. Phys. **43**, 163001 (2010).
[66]G. van Miert and C. Ortix, "On the topological immunity of corner states in two-dimensional crystalline insulators," npj Quantum Mater. **5**, 63 (2020).
[67]M. Jung, Y. Yu, and G. Shvets, "Exact higher-order bulk-boundary correspondence of corner-localized states," arXiv:2010.10299.